Eur. Phys. J. D **35**, 341–348 (2005)
DOI: 10.1140/epjd/e2005-00214-6

THE EUROPEAN PHYSICAL JOURNAL D

CO dynamics induced by tunneling electrons: differences on Cu(110) and Ag(110)

N. Lorente[1,2,a] and H. Ueba[2]

[1] Laboratoire Collisions, Agrégats, Réactivité, UMR 5589, IRSAMC, Université Paul Sabatier, 118 route de Narbonne, 31062 Toulouse Cedex 4, France
[2] Department of Electronics, Toyama University, Toyama 930-8555, Japan

Received 30 March 2005
Published online 2nd August 2005 –

Abstract. The electronic current originating in a scanning tunneling microscope (STM) can be used to induce motion and desorption of adsorbates on surfaces. The manipulation of CO molecules on noble metal surfaces is an academic case that has received little theoretical attention. Here, we do thorough density functional theory calculations that explore the chemisorption of CO on Cu(110) and Ag(110) surface and its vibrational properties. The STM induced dynamics are explored after excitation of the highest lying mode, the C–O stretch. In order to give a complete account of this dynamics, the lifetime of the different CO modes is evaluated (by only including the mode decay into electronic excitations of the host surface) as well as the intermode coupling. Hence, after excitation of the stretch mode, the lower-energy modes are populated via intermode coupling and depopulated by electron-hole excitations. This study reveals the intrinsic features of the STM induced motion of CO on Cu(110) and Ag(110).

PACS. 68.37.Ef Scanning tunneling microscopy (including chemistry induced with STM) – 68.43.Pq Adsorbate vibrations

1 Introduction

The scanning tunneling microscope (STM) has proven to be a versatile tool. Not only can it map solid surfaces at atomic resolution [1], but it can also induce adsorbate motion [2], break bonds [3], catalyze reactions [5], create bonds [4] and measure the vibrational spectra of chemisorbed species [6]. This versatility can be traced back to the tunneling character of the electronic current. Tunneling from virtually an atomically-finished metallic tip leads to electron beams with sub-Ångström localization. Besides its unique localization, tunneling confers the STM with extremely controllable low electron fluency. Hence, not only can the electron beam be directed with enhanced precision, but it can also be dosed at extremely weak currents. A third controllable parameter is the tip-sample bias voltage. This gives a handle on the quantum of energy transferable to the sample. These characteristics permit to give controlled doses of energy locally, hence opening the door to systematic studies of vibration induced motions [7] and vibrationally selected dynamics [8].

Tunneling currents have been used to desorb CO molecules from Cu(111) [9]. The tip-substrate voltage had to reach 2.4 V in order to induce any measurable desorption. By comparing their experimental findings with theoretical [10] and their own two-photon photoemission results [9], the authors conclude that desorption takes place by driving 0.05% of the tunneling current through the CO-induced $2\pi^*$ resonance. At lower voltages, migration of CO molecules on metallic surfaces is possible [7]. In this case, the $2\pi^*$ resonance remains inaccessible to the tunneling electrons. Instead, the exciting mechanism is vibrational in character. When the CO stretch mode I is excited by tunneling electrons, intermode coupling efficiently transfers energy from the stretch coordinate into translation reaction pathways. This has been clearly shown in the case of CO chemisorbed on Pd(110) [7]. Surprisingly, the same strategy yields no motion of CO adsorbates on Cu(110). This finding was rationalized in terms of the large number of quanta of the frustrated translation mode, T, in order to match the energy of the translational barrier [7,11].

The excitation of CO vibrations on metallic surfaces has been achieved by different groups [12–14]. The variation of conductance over each vibrational threshold is used to detect the excitation of the molecular modes [6, 12–14]. On Cu(110) surfaces, only the C–O stretch mode, I (measured frequency 257 meV [12]), and the frustrated rotation one, R (measured frequency 36.3 meV [12]), have been detected. These results show that tunneling electrons are indeed efficient in exciting the stretch mode, I. The R mode is also detectable on Ag(110) surfaces [4]

[a] e-mail: lorente@irsamc.ups-tlse.fr

(measured frequency 19 meV [4]). However, the migration of CO molecules took place with 100% efficiency whenever the tip-substrate bias voltage reached beyond 0.25 V, making it impossible to detect the I mode [4]. This behavior is somewhat reminiscent of the one found on Pd(110) as compared to Cu(110) surfaces [7]. In Pd the d-electron band is pinned at the Fermi energy, while it is fully filled in Cu (at some 2 eV below the Fermi level). This is a qualitative difference that shifts the interactions energies, the barriers and the molecular frequencies between both surfaces. As shown in reference [11], it is the harder frustrated translation, T, mode that sets the difference between the migration of CO on Pd and Cu surfaces.

The comparison of Ag(110) and Cu(110) surfaces is less contrasted than in the previous case. Ag is also a noble metal, with the d-band at some 3 eV below the Fermi level. In principle, the case of Ag as compared with Cu, is the opposite of Pd, and yet, CO migration is also very efficient. In order to understand this puzzling experimental result, we have undertaken density functional calculations of CO on both surfaces, we have evaluated its vibrational properties, and we have calculated the CO mode lifetimes following the theory developed in reference [15] and the intermode coupling rates [16,17]. The aim of the present work is to elucidate the reaction path after excitation of the I mode, comparing the lifetimes and different probabilities on both surfaces with the same degree of accuracy.

The outline of the paper consists of the description of CO chemisorption on Cu(110) and Ag(110) which includes total energies, geometrical data, electronic structure in terms of molecular orbital hybridization and a discussion of the precision of the calculation and the actually valuable data. This section will be followed by the description of the vibrational structure of CO on Cu(110) and Ag(110), again the results will be confronted against existing experimental data and an assessment of the accuracy of the present results. Lifetimes of the four molecular modes will be analyzed in the third section, and the intermode coupling rates will be given and discussed in the last section. We will conclude the paper with a summary and brief analysis of STM-induced migration of CO molecules on Cu(110) and Ag(110) at very low bias voltage.

2 Chemisorption of CO on Cu(110) and Ag(110)

The chemisorption of CO on Cu(110) and Ag(110) has been studied by density functional (DF) calculations. We have used the pseudopotential planewave code `Dacapo` [18,19]. In reference [19] a complete study of CO chemisorption on different transition metal substrates is carefully described together with a detailed analysis of the calculation process.

We have followed reference [19], and adapted the actual parameters of the calculation to the present case. The (110) surfaces have been approximated by slabs of 6 atomic layers, plus 5 vacuum atomic layers. The 3 first layers have been fully relaxed in the presence of dipole

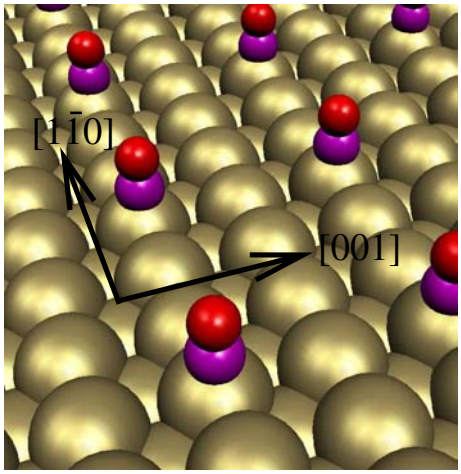

Fig. 1. Array 2×3 of CO molecules chemisorbed on Cu(110) or Ag (110). The C atom is between the O and the metal atom. The [1$\bar{1}$0] direction proceeds along the troughs of the surface, while the [001] direction is perpendicular to the troughs. A colour version of the figure is available in electronic form at `http://www.eurphysj.org`.

corrections. Then, one molecule of CO is introduced in a surface periodic pattern 2×3 as shown in Figure 1. We expect that this adsorbate density is low enough to approximate single adsorbate properties. The molecules and the 3-first atomic layers are again relaxed in the geometry of Figure 1, until the maximum force is smaller than 0.01 eV/Å. This good convergence in forces is important for the vibrational studies. The CO molecule is sitting ontop of a Cu or Ag atom with the C atom between the metal and the O atoms. As shown in reference [19] the C and O pseudopotentials are critical for a precise study. Here we are using rather soft pseudopotentials [20], with a cutoff of 26 Ry, this will certainly limit the precision that we can attain. We have tested that a $4\times4\times1$ k-point sampling gives converged total-energy results (the chemisorption energy changes less than 5%), this is not the case in all of the studies of the following sections where we have used a $6\times6\times1$ k-point sampling. The exchange and correlation functional is approximated by the PW'91 of the generalized gradient approximation [21]. This choice of functional is due to the overall good properties of the PW'91 at describing both molecular and solid geometries. Nevertheless other functionals have proved their superiority in chemisorption energy evaluations [19].

The ultrasoft pseudopotentials used for Cu and Ag give bulk lattice parameters of 3.66 Å and 4.14 Å respectively (roughly 1% larger than the experimental ones). Upon chemisorption the C–O distance expands from the free-molecule value, 1.16 Å, to 1.17 Å. This interatomic distance is quite constant regardless of whether the studied surface is Cu or Ag. Indeed the C–O interatomic difference between both substrates is only of 0.003 Å. This value compares very well with the C–O interatomic distance on Cu(100) of 1.18 Å [22]. However it is 0.02 Å shorter than the one reported in reference [19], this difference is probably due to the different pseudopotentials used for C and

Table 1. Geometrical results of CO chemisorption on Cu(110) and Ag(110). All distances are between atoms and given in Å. The last row is the vertical displacement of the metallic atom below the C atom.

distance (Å)	Cu(110)	Ag(110)
C–O	1.166	1.163
C-Metal	1.860	2.081
ΔZ Metal	0.128	0.049

O. Due to the surface relaxation, the metal atom is vertically pulled out of the surface plane by 0.13 Å for the Cu(110) surface and 0.05 Å for the Ag(110). This finding reflects what is going to be from now on the constant result of our calculations: CO interacts more strongly with the Cu(110) surface than with the Ag(110) one [23].

Our calculations predict an upward configuration of the CO molecule on both surfaces. Although this is well known for CO chemisorption on Cu surfaces, there has been some discussion on the literature about the actual configuration of CO on Ag surfaces. Initial photoelectron measurements led to the conclusion that the CO axis was not upright on Ag(110) [25]. More recent EELS measurements seem to indicate that at very low coverages CO on Ag(110) lie parallel to the surface, and it acquires the conformation found in our calculations when the coverage increases [26].

Table 1 shows the comparison between the chemisorption geometries on Cu(110) and Ag(110). As we announced above, the CO interaction with Ag is smaller, leading to a C–O interatomic distance closer to the free-molecule one, a C–Ag distance larger than the C–Cu and to a smaller buckling of the Ag surface. The chemisorption energies also show this trend. The computed chemisorption energy is defined as the difference between the total energy of the full system minus the sum of the free molecule and the free surface. For Cu(110) we find -0.95 eV, to be compared with the experimental result of -0.63 eV [27], and for Ag(110) we find -0.45 eV against the experimental value of -0.24 eV [28]. The appreciable difference between computed and experimental values can be traced back to the exchange and correlation potential, and the C and O pseudopotentials. Indeed, for better converged values, hard pseudopotentials are needed. Hammer et al. [19] show that already a 0.12-eV difference can come from using a harder O pseudopotential. Geometrical data are in better agreement with experiment. Indeed, molecular interatomic distances are in almost perfect agreement with experiments, as well as bonding angles [15].

The failure of the exchange and correlation functional in the description of CO chemisorption has been thoroughly analyzed in references [29,30]. The situation is quite critical, since all common local and semilocal (generalized gradient) approximations fail to give the correct chemisorption site. In the case of Cu(110) we have forced the on-top configuration of Figure 1, but our calculations give higher coordination sites as preferable as is found in references [29,30] for other transition metal surfaces. On the contrary, the calculated chemisorption energy is lowest for the on-top position of the Ag(110) surface. This finding is significant and can be rationalized in terms of the electronic structure of the CO-Metal bond. Indeed, silver's *d*-electron band is lower in energy, reducing considerably its overlap with the molecular orbitals of CO. This leads to a stronger interaction with the extended *sp*-band than in the case of Cu(110). For the latter, the interaction with the *d*-band dominates the binding of the molecule, trying to optimize the molecule-*d*-band overlap.

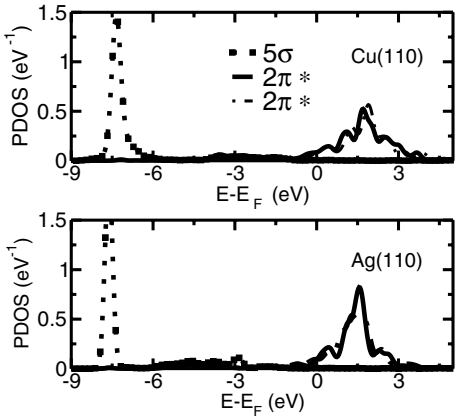

Fig. 2. Projected density of states on the 5σ, and two $2\pi^*$ molecular orbitals of CO on Cu(110) and Ag(110). The stronger interaction of CO on Cu leads to a small upward shift of the molecular electronic energy levels and, more importantly, to broader features, indicating shorter lived electronic resonances. In order to represent these peaks, a numerical Gaussian broadening of 0.2 eV has been used.

Charge transfer can be qualitatively accounted for in our calculations by performing projected density of states (PDOS) [15,31]. Briefly, the PDOS is one way of evaluating how much of molecular character the electronic structure of the chemisorbed system retains. Let $|\mathrm{MO}\rangle$ be a molecular orbital state MO, calculated for the free molecule with the geometry of the chemisorbed one (in order not to have geometrical artifacts), let the fully chemisorbed system have the states $|\mu\rangle$ with Hamiltonian eigenvalues ϵ_μ, then the PDOS at a given energy E on the MO is:

$$PDOS(E) = \sum_\mu |\langle \mathrm{MO}|\mu\rangle|^2 \delta(E-\epsilon_\mu). \qquad (1)$$

This equation gives the weight in MO of the different states at a given energy. In the case of a MO in front of a structureless electronic continuum, equation (1) gives a Lorentzian since the MO becomes a Breit-Wigner resonance. The PDOS is a very useful quantity because it permits the description of the full electronic structure in terms of the molecular one.

Figure 2 gives the PDOS projected on the 5σ, and the two $2\pi^*$ of the CO molecule. We see that the peak originating in the 5σ projection is very narrow, showing the small hybridization of the 5σ MO with the substrate electronic wave functions. On both substrates we see that the 5σ PDOS increases at the energies of the *d*-band, indicating

some hybridization with the d-electrons of the substrate. We can also see that the tail above the Fermi level of the 5σ PDOS is negligible, which indicates very little donation from the molecule into the substrate. The $2\pi^*$ MO's are closer to the Fermi level and present a stronger distortion, leading to the larger width of the $2\pi^*$ peaks, and charge transfer into the molecule as seen in the tail developing below the Fermi energy. Indeed, these calculations show the dominating role of charge transfer from the surface into the $2\pi^*$. This PDOS-based analysis runs along the argumentation behind the Blyholder model [32]. The comparison between both surfaces leads to the conclusion that indeed the interaction is stronger for the Cu substrate. We see that the electronic structure is shifted upwards with respect to the Ag substrate and, more importantly, the electronic structure presents broader features, signal of a stronger interaction. We can conclude that charge transfer into the CO on Cu(110) is larger.

This conclusion agrees well with the C–O interatomic distances found in Table 1. Indeed, we see that on Cu(110) the C–O distance is slightly larger, in agreement with a larger population of the antibonding $2\pi^*$ orbitals. In the same direction, we have evaluated the change in work function due to the induced dipole during chemisorption. Even at the small coverage of the calculations, we find appreciable work function changes. For Cu(110) the work function change is 0.16 eV, positive, indicating an increase of work function and hence an overall negative dipole on the surface. For Ag(110) the change is 0.03 eV, also positive. We see that the work function change in Cu(110) cannot be explained with the intrinsic dipole of CO alone, but one needs to make use of the population of the $2\pi^*$ resonances in order to have the correct dipole variation.

These results show that the interaction of CO with Cu(110) is much larger than on Ag(110) basically because of the 1 eV of upward shift of the d-electron band of Cu with respect to Ag. Indeed, the interaction on Ag(110) is small (the experimental chemisorption energy is -0.24 eV), and we can expect that the translational barriers will follow the same trend and be much lower than in the case of Cu(110). Unfortunately, as stressed above, the present state of DFT calculation does not permit the accurate evaluation of barriers for these systems.

3 CO vibrational modes on Cu(110) and Ag(110)

Despite the deficiencies of DFT to account for the chemisorption energies of CO on transition metal surfaces, the local quantities are probably more correctly taken care of. Indeed, recent calculations show that both vibrations and work functions changes are significant even in the case of physisorbed species where DFT fails most notoriously [33]. The calculation of vibrations seems to be particularly robust against artefacts of the different models that are used. Bauschlicher [34] shows that the vibrational frequencies are quite independent of system sizes and electron correlation, that are very important for chemisorption energies.

Table 2. Vibrational modes of CO on Cu(110). The first column is the CO mode: I for the C–O stretch, M for the center of mass stretch, R for the frustrated rotation mode where the C and O atoms move parallel to the surface but with opposed phases, and T for the frustrated translation mode where the parallel motion of both atoms is in phase. The second column is the mode frequency in meV. The third column is the direction of the motion; Z for perpendicular to the surface, X along the [001] direction (see Fig. 1) and Y along the $[1\bar{1}0]$ direction. The three following columns give the atomic displacement of the C, O, and Cu atom respectively in Å.

	$\hbar\omega$ (meV)	direction	C (Å)	O (Å)	Cu (Å)
I	260.9	Z	−0.0198	0.0142	0.0002
M	49.5	Z	0.0307	0.0326	−0.0147
R	38.0	Y	0.0580	−0.0294	−0.0030
R	35.6	X	0.0600	−0.0275	−0.0034
T	7.7	X	0.0708	0.1145	0.0031
T	7.1	Y	0.079	0.1157	0.0031

Table 3. Vibrational modes of CO on Ag(110). The columns correspond to the columns of Table 2.

	$\hbar\omega$ (meV)	direction	C (Å)	O (Å)	Ag (Å)
I	261.5	Z	0.0196	−0.0145	0.0000
M	33.3	Z	0.0406	0.0414	−0.0118
R	28.7	X	−0.0749	0.0171	0.0002
R	25.5	Y	−0.0714	0.0346	−0.0004
T	9.1	X	0.0349	0.1153	0.0022
T	8.0	Y	0.0720	0.1103	0.0030

The calculations are performed by computing the dynamical matrix with finite differences. Practically, this implies to produce finite displacement of each of the considered atoms, evaluate the forces on the rest of the moving atoms, and repeat the operation until all active atoms have been displaced along the 3-spatial coordinates. Finite displacements are better behaved when performed in centered differences, this means that typically 6 displacement are effected per atom. The size of the displacement is also important. In the present work, we have tried to optimize the low-energy modes of the molecule. In order to do this, we have used different finite increments for the CO and for the metallic surface. For CO we have used up to 0.1-Å displacements. The root mean square displacement is inversely proportional to the square root of the frequency, hence the smaller the frequency the larger the mode motion. In Tables 2 and 3 we give the full data of the molecular modes. In particular, columns 4, 5 and 6 are the root mean square displacements of the mode on each atom. We find that the frustrated translation, T, mode leads to displacements of ∼0.1 Å of the CO atoms. However the metallic atoms present smaller displacements. We have evaluated the dynamical matrix by performing 0.03-Å displacements of the metal atoms.

Only the first surface layer of metallic atoms have been made active in the dynamical matrix. The reason to do so is that we expected that the molecule would

perturb the metallic surface during its vibrations. Again the T mode may seem to be the most affected by the surface motion. Indeed, it is resonant with both surface's phonon bands [24]. The effect of the T resonance is that the surface phonon continuum gives a finite lifetime to the T mode as well as a shift of frequencies. Lewis and collaborators [35,36] have studied the T resonance. This has permitted them to find a strong damping of the T vibration via coupling with metallic phonons. At 0.5 CO coverage, the lifetime of the T mode can be basically associated with the damping by bulk Cu phonons [35].

In principle, the coupling with the phonon continuum will also shift the resonant frequencies. However, Lewis and collaborators [36] show that the renormalization factor of the T mode on Cu(100) is 0.956, and hence the intrinsic error of our finite-differences method will already be larger.

The C–O stretch, I, is considerably downshifted to ∼260 meV (from the gas phase value of 269 meV). This is consistent with the elongation of the C–O distance and the weakening of the bond by charge capture into the antibonding $2\pi^*$ resonances. These results are in good agreement with the available experimental data. The I mode on Cu(110) has been measured with the STM [12] to be 257 meV and 259 meV as measured with IRAS [37]. On Ag(110), HREELS measurements yield 261 meV [38]. As we noted in the introduction, this mode has not been measured with the STM because the inelastic current makes the molecule hop away from the tip.

The center-of-mass mode, M, involves the motion of the metal atom below the C atom. As we can see in Tables 2 and 3 the displacement of the metal atom corresponds to a large fraction of the motion of both the C and the O atoms. Rather than for the T mode, the inclusion of the surface atoms is fundamental to account for the correct frequencies of the M mode. The M mode presents considerable softening on the silver surface. This is not surprising after the conclusions of Section 2, where we showed that the CO-metal interaction is much weaker on silver, and that the M mode is governed by this interaction.

The frustrated rotation, R, mode has a much smaller component of the metal atom, and is roughly above the surface phonon band. On Cu(110) we obtain very good agreement as compared with the experimental value of 36.3 meV measured with the STM [12]. However, the agreement with experiment of the same mode on the silver surface is considerably worse. On Ag(110) the experimental value is 19 meV [4] while the calculated mode is at least 5 meV higher. This result might be a consequence of trying to optimize the finite displacement in the dynamical matrix calculation for the T mode. Indeed, reducing the displacement to 0.05 Å leads to better agreement with the experimental values. The calculated R modes seem to be very sensitive to the anisotropy of the (110) surface. We obtain mode splittings along the X- and Y-directions (see Tabs. 2 and 3) of the order of 3 meV. This is somewhat a troubling result, because it means that the local chemisorption potential may be affecting the description of the R mode, and as we showed in Section 2, DFT is not correct in accounting for this kind of information.

The T mode has received a lot of attention given its influence in the diffusion of the molecule. Our calculations yield 7.7, X-direction and 7.1 meV, Y, for the Cu(110) surface, while experimentally the mode is found at 3.2, X, and 3.6 meV, Y [39]. Besides the large error bar, we notice that the directions of the softer mode and the harder one are opposite. Moreover, a thorough experimental analysis of the T mode on Cu(100) [40] shows the need to consider an anharmonic quartic potential in order to obtain the correct frequency and damping of the T mode. Given these facts, our calculations are, at best, educated guesses of the T modes.

4 Lifetimes of CO modes on Cu(110) and Ag(110)

The computation of the vibration's lifetimes is much more robust than the calculation of the vibrational frequencies itself. The actual reason is rather that for a "good" lifetime calculation, the order of magnitude basically *suffices*, while for mode calculations we can generally be better than 5% at least for the high-lying modes. The calculation as implemented here follows the work of references [15,17], and for the formulation and computational details we direct the reader there. The theory here and in reference [15] is a periodic array (planewave code) implementation of the cluster calculation by Head-Gordon and Tully [41]. Briefly, we use Fermi Golden rule to compute the vibration lifetime due to coupling with the electronic excitations of the full surface-molecule system [17]. Since, we are dealing with a periodical array of molecule and metallic atoms, the eigenfunctions of the Hamiltonian are Bloch states $|n\mathbf{k}\rangle$ where n is the band index and $\mathbf{k}$ the wave vector of the Brillouin zone, hence the lifetime is expressed as [15,17]:

$$\frac{1}{\tau} = \frac{2\pi}{\hbar} \sum_{n,m,\mathbf{k}} (1 - f_m) f_n \times |\langle m\mathbf{k}| \frac{\partial \hat{H}}{\partial \mathbf{Q}_\lambda} \cdot \delta\mathbf{Q}_\lambda |n\mathbf{k}\rangle|^2 \times \delta(\epsilon_{m,\mathbf{k}} - \epsilon_{n,\mathbf{k}} - \hbar\omega_\lambda). \quad (2)$$

Where $\mathbf{Q}_\lambda$ is the eigenvector of the dynamical matrix for the mode λ, normalized to the root mean squared displacement of the mode, and $\hat{H}$ is the full adiabatic Hamiltonian. The electron-vibration coupling is then given by $(\partial\hat{H}/\partial\mathbf{Q}_\lambda) \cdot \delta\mathbf{Q}_\lambda$ which does not mix different k-points $\mathbf{k}$, but only electronic states of different band index $n \rightarrow m$ while exchanging one quantum of vibration $\hbar\omega_\lambda$. The Fermi factors f_m and f_n take care of the occupation of the states, n corresponding to an occupied states and m to an empty one, hence the name of electron-hole excitation.

We would like to emphasize that in this periodic array calculations the k-point sampling is critical. As a matter of fact going from a $4 \times 4 \times 1$ to a $6 \times 6 \times 1$ k-point

Table 4. Lifetimes of CO vibrations due to electron-hole damping [15,17,41]. The error bar of the calculation is the uncertainty due to the number of electronic states taken in the broadening of the δ-function by a Gaussian of width σ ranging from 0.1 eV to 0.4 eV, in equation (2).

	Cu (110) ($\times 10^{12}$ s^{-1})	Ag (110) ($\times 10^{12}$ s^{-1})
I	0.45 ± 0.03	0.53 ± 0.03
M	0.093 ± 0.005	0.137 ± 0.005
R	0.37 ± 0.05	0.33 ± 0.05
T	0.013 ± 0.001	0.008 ± 0.001

sampling in this 2×3 surface supercell can mean changing the lifetime by a factor of 3. We try to do better than that. Together with the convergence in k-point, the δ-function convergence is important. In order to represent the energy conservation via the δ-function of equation (2), we use a Gaussian of width σ such that in the limit $\sigma \to 0$ we recover a δ-function. When the calculations are converged in k-points, the density of considered electronic states is large enough to find small variations of the final results of equation (2) as σ changes. In the present work, we have used $\sigma = 0.25$ eV. And we have estimated the error bar in the calculation by varying σ from 0.1 eV to 0.4 eV.

Table 4 presents the results of the different mode lifetimes on Cu(110) and Ag(110). The general trend that we find is that the "harder" modes (I and M) are slightly more damped on Ag(110) than on Cu(110), while the "softer" modes (R and T) are slightly more damped on Cu(110). This trend is due to the symmetry of the modes. I and M are longitudinal modes that only couple electronic states with the same symmetry with respect to the 2 perpendicular planes containing the molecules axis. Hence the I mode couples Bloch states that basically contain contributions either from the $2\pi^*$ resonance or the 5σ. The R and T mix electronic states of different symmetry, for example they will couple states with $2\pi^*$ symmetry with states of 5σ. When we look at the electronic structure analysis contained in Figure 2, we realize that the stronger interaction on the Cu surface, hybridizes more the molecular and surface states, leading to broader features which favors the contribution of states sharing different molecular symmetries.

The lifetime basically follows the trend marked by the mode's frequency. Indeed the damping is largest for the I mode, then the M and finally the T. This behavior can be understood if we assume constant electron-vibration couplings, then the available phase-space of electron excitation is given by $\hbar\omega_\lambda$. However, the R mode presents an electron-hole damping almost as large as the I mode. This is due to the very large electron-vibration coupling of the R mode, as has been seen in STM vibrational spectroscopy and in various studies of electron-vibration interactions in CO [12,15,41].

The electron-vibration damping does not seem to be extraordinarily affected by the actual surface orientation, but rather by the local type of bonding to the surface. Indeed, the damping rates obtained for the Cu(100) surface [15] or recent calculations on the Cu(111) [42] are in excellent agreement with the results presented here.

As we advanced in Section 3, the lifetime of the T mode is determined by its resonant character with the surface phonon bands. At 0.5 monolayer coverage, the "bulk" phonon counts for most of the coupling of the localized vibration with the extended phonons [35]. However, as the coverage is reduced, the electron-vibration contribution becomes more important. Measurements of the lifetime of the T mode on Cu(100) at low coverage [40] give a vibrational lifetime of 8 ps for the isolated molecule extrapolation. Our calculations give 77 ps, showing that the vibration-phonon coupling is still the lifetime limiting factor even at very low coverage.

5 Intermode coupling in CO modes on Cu(110) and Ag(110)

The migration process of CO molecules on Pd(110) [7] is initiated by the excitation of the I mode. As shown in reference [11], it is the intermode coupling of this mode with the T mode that permits the eventual transition of the translational barrier. The large mismatch in energies between the I and the T modes on Cu(110) make very unlikely the transition. Experimental measurements [43] yield a translational barrier of 97±4 meV for CO molecules on Cu(110) along the $[1\bar{1}0]$ direction. The experimental T-mode frequency is ∼4 meV, hence the overcoming of the barrier needs in the range of 25 quanta of excitation. The same estimation yields 6 quanta for the Pd(110) case [7]. This is the main difference between overcoming or not a barrier by intermode coupling.

In reference [11], the intermode coupling due to anharmonicities of the potentials is considered. In the present section however, we are going to study the intermode coupling in the harmonic regime. This means that only single-quantum excitations are considered. The aim of the present section is to evaluate how likely intermode coupling is due to the excitation of electron-hole pairs, and what information can be extracted on the motion of CO on Cu(110) and Ag(110). Hence, the theory follows the same line of reasoning as the calculations shown in Section 4.

The I to T intermode coupling rate [17] is again calculated using Fermi's Golden rule:

$$\frac{1}{\tau_{I,T}} = \frac{2\pi}{\hbar} \sum_{m,n,\mathbf{k}} f_n(1-f_m) \times |\langle 1,0,m|\delta\mathbf{Q}_I \cdot \frac{\partial^2 H}{\partial \mathbf{Q}_I \partial \mathbf{Q}_T} \cdot \delta\mathbf{Q}_T|0,1,n\rangle|^2 \times \delta(\epsilon_m - \epsilon_n + \hbar\omega_I - \hbar\omega_T). \quad (3)$$

The difference of equation (2) with equation (3) lies in the electron-vibration coupling that now depends on the two normal-mode sets of coordinates, $\mathbf{Q}_I$ and $\mathbf{Q}_T$. The second derivative is again calculated by finite differences [17]. The combined electronic and nuclear states are initially the I-mode one time excited and the electron in the occupied

Table 5. Intermode coupling rates of the CO I-mode with the lower lying modes via electron-hole excitation [17]. The error bar of the calculation is the uncertainty due to the number of electronic states taken in the broadening of the δ-function by a Gaussian of width σ ranging from 0.1 eV to 0.4 eV, in equation (3). The intermode rates should be multiply times two to take into account the *quasi* degeneracy of the T and R modes.

	Cu (110) ($\times 10^{10}$ s^{-1})	Ag (110) ($\times 10^{10}$ s^{-1})
M	0.15 ± 0.02	0.26 ± 0.02
R	1.1 ± 0.2	1.2 ± 0.2
T	0.148 ± 0.004	0.085 ± 0.004

state n, as given in the ket $|0, 1, n\rangle$, and the final state is the T-mode once excited and the electron in the unoccupied state m, as given in the bra $\langle 1, 0, m|$.

Table 5 shows the results of the intermode coupling rates between the I mode and the rest of the CO modes, obtained with the same calculation parameters of Section 4. We obtain that only for the coupling with the M mode on the Ag(110) surface, the intermode coupling is larger than on the Cu one. The explanation is the same as in Section 4, because both coupled modes have the same longitudinal symmetry and do not couple electronic states with different molecular character. Again the R and T modes couple electronic states of different symmetries, here the larger interaction on the Cu surface, mixes the molecular and metallic states more efficiently leading to a larger density of states available for the electronic transitions. Here the differences are not as large as for the lifetimes because we also need to have an important contribution coming from the I mode that couples states with the same symmetry, and thus favors the Ag substrate.

The R-mode has again the largest coupling, given again, see Section 4, by the very large electron-vibration coupling when the R-mode is involved in an electronic transition. All these and other calculations [15,42] show the very large contribution of the R mode. This strength of the R-mode coupling make us think that the R mode may have a leading role in the dynamics of CO motion on metallic surface that has not been considered until now.

The computed intermode couplings, Table 5, show very little difference between the two substrates. The conclusion is that the mechanism differentiating the migration of CO on Cu(110) (no motion [7]) and on Ag(110) (very efficient motion [4]) does not have its origin in the intermode coupling strength. Rather it points again to the interpretation given in references [7,11]. Our calculation yield similar frequencies for the T modes, Section 3, but the CO-metal interaction is more than twice as large on the Cu(110) than on the Ag(110) surfaces, Section 2. It is natural to assume that there would be about half of excited quanta in the translation on Ag(110) as compared to translation on the Cu(110). Nevertheless these calculations do not permit to clarify this point due to the unavailability of computations of translational barriers for these systems.

6 Conclusions

The present work deals with DFT calculation as performed with the pseudopotential planewave code `Dacapo` [18]. We have used a periodic array of upright CO molecules sitting on-top of metallic atoms every 2×3 surface atoms. Besides the incapability of present implementations of DFT to yield the correct chemisorption energies of CO on transition-metal surfaces, we can obtain valuable information comparing the different chemisorption parameters and electronic structure of CO on Cu(110) and Ag(110). Our conclusion is that the interaction on Cu(110) is much stronger, as seen by chemisorption energies that are more than twice as large on the Cu surface, and by the much more hybridized molecular electronic structure on the Cu surface. The reason for this quite different behavior is the difference in the band edge of the surface d-electrons. For Cu(110) the band lies $\sim$1 eV higher than for Ag(110), presenting larger overlap and interaction with CO's molecular orbitals.

Our calculations permit to obtain the frequencies of the different modes of the surface. We have tried to improve the description of the frustrated translation, T, modes. In order to do so, we have optimized the finite-difference increment and we have allowed the surface atoms to move. The shift of frequencies of the T-mode due to the coupling with the substrate modes is negligible [35], but we find an important contribution from the surface to the center-of-mass mode, M. Despite our efforts, our frequencies accumulate an error of 50% for the T mode, but 1% for the C–O stretch, I mode. The failure to give a more accurate T mode is due to the quartic anharmonicity of this mode [40], hence calculations based in the harmonic approximation, as the present one, cannot claim a better accuracy.

We have calculated the lifetime of the CO modes on Cu(110) and Ag(110). We find slight differences between the two substrate. On Ag(110) the harder modes present shorter lifetimes while on Cu(110) the softer modes are more efficiently damped by electron-hole excitation. This finding has been rationalized in terms of the symmetry of the modes and the CO-metal electronic structure.

Using a similar approach, we have evaluated the harmonic intermode coupling of the I mode with the lower lying modes. We find a similar behavior as for the lifetimes, which can be understood in terms of electronic structure and mode symmetries. Both for the damping rates and for the intermode coupling rates, we find the predominance of the frustrated rotation, R, mode on both substrate. We assign this to the very large electron-vibration coupling of the R mode and not to an effect of excitation phase space that easily explains the qualitative behavior of the same quantities for the other modes.

The motivation behind this work was to shed light on the motion of CO molecules on Ag(110) above the 250 mV threshold [4], and the immobility of CO on Cu(110) [7]. The similarity of lifetimes and intermode coupling on both substrates leads us to assign the difference to the very different strength of the CO-metal interaction, and not to a difference in electron-vibration and intermode couplings.

N.L. acknowledges Japan Society for the Promotion of Science (JSPS) for a Research Fellowship for Young Scientists (No. PE04024) and the hospitality of Toyama University. H.U. was also supported by a Grant-in-Aid for Basic Research (No. 15310071) from JSPS. Computational resources at the Centre Informatique National d'Enseignement Supérieurs and the Centre de Calcul Midi-Pyrénées are gratefully acknowledged.

References

1. G. Binnig, H. Röhrer, C. Gerber, E. Weibel, Phys. Rev. Lett. **49**, 57 (1982)
2. D.M. Eigler, E. Schweizer, Nature **344**, 524 (1990)
3. G. Dujardin, R.E. Walkup, Ph. Avouris, Science **255**, 1232 (1992); B.C. Stipe, M.A. Rezaei, W. Ho, S. Gao, M. Persson, B.I. Lundqvist, Phys. Rev. Lett. **78**, 4410 (1997)
4. H.J. Lee, W. Ho, Science **286**, 1719 (1999)
5. B.J. McIntyre, M. Salmeron, G.A. Somorjai, Science **265**, 1415 (1994)
6. B.C. Stipe, M.A. Rezaei, W. Ho, Science **280**, 1732 (1998)
7. T. Komeda, Y. Kim, M. Kawai, B.N.J. Persson, H. Ueba, Science **295**, 2055 (2002)
8. J.I. Pascual, N. Lorente, Z. Song, H. Conrad, H.-P. Rust, Nature **423**, 525 (2003)
9. L. Bartels, G. Meyer, K.-H. Rieder, D. Velic, E. Knoese, A. Hotzel, M. Wolf, G. Ertl, Phys. Rev. Lett. **80**, 2004 (1998)
10. M.-L. Bocquet, P. Sauter, Surf. Sci. **360**, 128 (1996)
11. B.N.J. Persson, H. Ueba, Surf. Sci. **502/503**, 18 (2002)
12. L.J. Lauhon, W. Ho, Phys. Rev. B **60**, R8525 (1999)
13. F. Moresco, G. Meyer, K.-H. Rieder, Mod. Phys. Lett. B **13**, 709 (1999)
14. J.I. Pascual, N. Lorente, in *SPM beyond imaging*, edited by P. Samori (Wiley-VHC, Berlin, 2005)
15. N. Lorente, M. Persson, Faraday Discuss. **117**, 277 (2000)
16. N. Lorente, J.I. Pascual, Phil. Trans. R. Soc. **362**, 1227 (2004)
17. N. Lorente, R. Rurali, H. Tang, J. Phys.: Condens. Matter **17**, S1049 (2005)
18. `Dacapo` is freely downloadable from: `http://www.fysik.dtu.dk/campos/ASE/`
19. B. Hammer, L.B. Hansen, J.K. Nørskov, Phys. Rev. B **59**, 7413 (1999)
20. D. Vanderbilt, Phys. Rev. B **41**, 7892 (1990)
21. J.P. Perdew, J.A. Chevary, S.H. Vosko, K.A. Jackson, M.R. Pederson, D.J. Singh, C. Fiolhais, Phys. Rev. B **46**, 6671 (1992)
22. C.J. Hirschmugl, G.P. Williams, F.M. Hoffmann, Y.T. Chabal, Phys. Rev. Lett. **65**, 480 (1990)
23. It is interesting to note that the Cu(110) surface phonons are harder than the Ag(110) one, indicating a stronger Cu–Cu interaction than in the Ag case, because the mass difference does not account for the phonon top of band distance (21 meV for the longitudinal modes of Cu against 13.7 meV of Ag(110) [24])
24. G. Bracco, R. Tatarek, F. Tommasini, U. Linke, M. Persson, Phys. Rev. B **36**, 2928 (1987)
25. S. Krause, C. Mariani, K.C. Prince, K. Horn, Surf. Sci. **138**, 305 (1984)
26. L.D. Peterson, S.D. Kevan, J. Chem. Phys. **95**, 8592 (1991)
27. J. Ahner, D. Mocuta, R.D. Ramsier, J.T. Yates, J. Chem. Phys. **105**, 6553 (1996)
28. U. Burghaus, H. Conrad, Surf. Sci. **338**, L869 (1995)
29. P.J. Feibelman, B. Hammer, J.K. Nørskov, F. Wagner, M. Scheffler, R. Stumpf, R. Watwe, J. Dumesic, J. Phys. Chem. B **105**, 4018 (2001)
30. G. Kresse, A. Gil, P. Sautet, Phys. Rev. B **68**, 073401 (2003)
31. R. Hoffman, Rev. Mod. Phys. **60**, 601 (1988)
32. C. Blyholder, J. Phys. Chem. **68**, 2772 (1964)
33. Y. Morikawa, H. Ishii, K. Seki, Phys. Rev. B **69**, 041403 (2004)
34. C.W. Bauschlicher, J. Chem. Phys. **101**, 3250 (1994)
35. S.P. Lewis, A.M. Rappe, Phys. Rev. Lett. **77**, 5241 (1996); S.P. Lewis, A.M. Rappe, J. Chem. Phys. **110**, 4619 (1999)
36. S.P. Lewis, M.V. Pykhtin, E.J. Mele, A.M. Rappe, J. Chem. Phys. **108**, 1157 (1998)
37. D.P. Woodruff, B.E. Hayden, K. Prince, A.M. Bradshaw, Surf. Sci. **123**, 397 (1982)
38. R.A. Pelak, W. Ho, Surf. Sci. **321**, L233 (1994)
39. J. Braun, J. Weckesser, J. Ahner, D. Mocuta, J.T. Yates, Ch. Wöll, J. Chem. Phys. **108**, 5161 (1998)
40. F. Hofmann, J.P. Toennies, Chem. Rev. **96**, 1307 (1996)
41. M. Head-Gordon, J.C. Tully, J. Chem. Phys. **96**, 3939 (1992)
42. M. Persson, Phil. Trans. R. Soc. **362**, 1173 (2004)
43. B.G. Briner, M. Doering, H.-P. Rust, A.M. Bradshaw, Science **278**, 257 (1997)